NANO LETTERS

2009
Vol. 9, No. 11
3914-3921

Tuning of an Optical Dimer Nanoantenna by Electrically Controlling Its Load Impedance

Johann Berthelot,[†] Alexandre Bouhelier,[*,†] Caijin Huang,[†] Jérémie Margueritat,[†] Gérard Colas-des-Francs,[†] Eric Finot,[†] Jean-Claude Weeber,[†] Alain Dereux,[†] Sergei Kostcheev,[‡] Hicham Ibn El Ahrach,[‡] Anne-Laure Baudrion,[‡] Jérôme Plain,[‡] Renaud Bachelot,[‡] Pascal Royer,[‡] and Gary P. Wiederrecht[¶]

Institut Carnot de Bourgogne, CNRS UMR 5209, Université de Bourgogne, 9 Avenue Alain Savary, Dijon, France, Institut Charles Delauney, Laboratoire de Nanotechnologie et d'Instrumentation Optique, Université de Technologie de Troyes, 12 Rue Marie Curie, Troyes, France, and Center for Nanoscale Materials, Argonne National Laboratory, Argonne, Illinois

Received July 3, 2009; Revised Manuscript Received August 24, 2009

ABSTRACT

Optical antennas are elementary units used to direct optical radiation to the nanoscale. Here we demonstrate an active control over individual antenna performances by an external electrical trigger. We find that by an in-plane command of an anisotropic load medium, the electromagnetic interaction between individual elements constituting an optical antenna can be controlled, resulting in a strong polarization and tuning response. An active command of the antenna is a prerequisite for directing light wave through the utilization of such a device.

Optical antennas are devices operating in the visible to infrared spectral region (for comprehensive review, see Bharadwaj et al.[1]) that offer technological solutions for developing ultrasensitive biological and medical tools,[2] increasing the efficiency of photonic interactions[3−5] and light extraction in solid state devices[6,7] and for engineering the radiation properties of single emitters[8−10] to name a few examples. Optical antennas are therefore likely to take a major role in the manipulation of light on the nanometer scale as they will be an intrinsic component of the building blocks used in optical nanoengineering. In turns, the use of optical antenna in functional integrated devices is strongly dependent on our ability to control electromagnetic radiation through the utilization of such a device. The characteristics of an optical antenna are generally inferred from its shape, material, and for multielements antennas, near-field interactions between individual constituants[6,11] and essentially remains a passive device. However, an on-demand external activation/control of an antenna is a highly desirable property to establish a controlled optical exchange between two nanoscale objects. Successful attempts to control the spectral resonances of ensembles of nanoparticles were demonstrated by reversible electrochemical and molecular switches.[12,13] Near-field coupling between antenna pairs were also precisely controlled mechanically[14,15] and photochemically.[16] Another class of material showing interesting properties in this context are electro-optical substances. Nematic liquid crystals (LC) for instance provide a simple strategy to create an active control of plasmonic responses[17,18] owing to their very large anisotropy ($\Delta n > 0.2$, where n is the refractive index). Individual spherical Au nanoparticles[19] and ensemble of Au nanorods[20,21] immersed in a biased LC cell unambiguously showed a voltage-dependent plasmonic response controlled by an out-of-plane reorientation of the crystal director. However and regardless of the original orientation of the director on the nanoparticles at a null bias, an out-of-plane switching of the LC molecules will reduce the anisotropy of the cell since for a normal incidence the electric field is traveling through constant index of refraction. The overall polarization anisotropy of the system is therefore governed by the anisotropy of the particles. On the contrary, an in-plane orientation of the directors introduces a polarization-sensitive index that can be superposed to the intrinsic anisotropy of a plasmonic optical antenna. In turns, this approach provides a much richer spectroscopic response of these devices and thus a higher degree of active control.

In this paper, we report on the voltage activation of the scattering spectrum of single dimer optical antennas. The control

* To whom correspondence should be addressed. E-mail: alexandre.bouhelier@u-bourgogne.fr.
[†] Université de Bourgogne and CNRS.
[‡] Université de Technologie de Troyes.
[¶] Argonne National Laboratory.

10.1021/nl902126z CCC: $40.75
Published on Web 09/14/2009

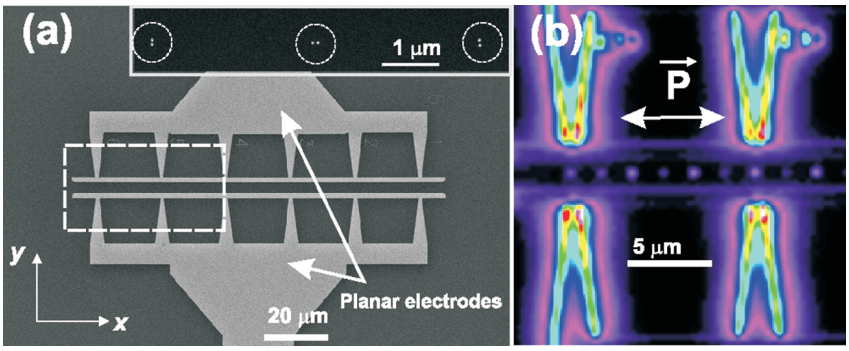

Figure 1. (a) Scanning electron micrograph of the sample layout. The microscopic planar Au electrodes are separated by a 3.5 μm gap. At the center of the gap, dimer optical antennas were fabricated by electron-beam lithography (dashed circle in the inset). Typical particle diameter is ~70 nm with interparticle distance varying stepwise from contact to 100 nm. The orientation of the dimer (parallel or perpendicular to the electrodes) is alternating for each antenna. (b) Dark-field optical microscope image of a selected area (boxed area in panel a) obtained for a linear polarization oriented along the electrodes. The optical antennas are readily visible in between the electrodes.

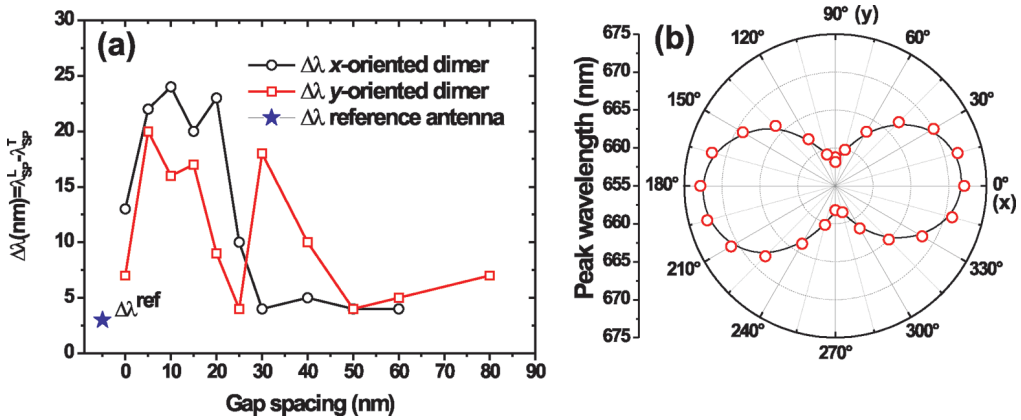

Figure 2. (a) Spectral difference between the longitudinal (λ_{sp}^{L}) and transverse (λ_{sp}^{T}) plasmon modes ($\Delta\lambda_{sp} = \lambda_{sp}^{L} - \lambda_{sp}^{T}$) for two type of orientations of the dimer's long axis as a function of the gap distance. The star data point corresponds to a reference antenna and consists of a single nanodisk element with a response independent of the incoming polarization. Significant hybridization of the resonances is observed for strongly interacting elements (gap size <30 nm). For the larger gap distance, the elements are not coupled and the response becomes isotropic. ($\Delta\lambda_{sp} \rightarrow \Delta\lambda^{ref} = 3$ nm). (b) Polar plot of the surface plasmon resonance (red circles) of a typical dimer antenna as a function of incident polarization. The solid line is a guide to the eyes.

is achieved by an in-plane index modulation of the anisotropic medium surrounding the optical antennas. We experimentally show that the optical index of the feed-gap region, that is, the load of the antenna,[22,23] plays an important part. We find an anomalous sensitivity of the devices to the incoming polarization and demonstrate an external control of the feed-gap load medium that in fine dictates the antenna response.

Gold nanoantennas were fabricated on a glass substrate by standard electron-beam lithography and lift-off techniques. The antennas were precisely placed between two microscopic planar electrodes separated by 3.5 μm, as shown by the scanning electron micrograph of Figure 1a. This median position insures that the electric field lines applied between the electrodes in the following are oriented in the plane. The devices were constituted of two interacting elements (nanodisks) forming a dimer antenna. The diameter and thickness of an element were approximately 100 and 50 nm, respectively. By design, the feed-gap between elements was systematically varied from contact to 100 nm. The pitch between dimer antennas was kept constant at 3 μm to ensure negligible mutual optical interactions between dimers. The orientation of the dimers alternates from a main axis parallel to the electrodes (x-direction) to an axis perpendicular to the electrodes (y-direction) as shown in the inset micrograph of Figure 1a. We do not have high-resolution micrograph of the antennas since electron charging at the glass substrate was strongly affecting the quality of the images. We used dark-field imaging to reveal the presence of the antennas as demonstrated by the false-color CCD image of Figure 1b. The electrodes are readily seen in the image. The area corresponds to the boxed area displayed in Figure 1a. Individual elements of the dimer antenna are not resolved in our apparatus due to the diffraction limit. Instead, dimer antennas are visible as luminous scattering elements centered between the two electrodes.

In a first step, we use dark-field spectroscopy to define the properties of the antennas in air. Figure 2a shows the spectral difference $\Delta\lambda$ between the resonance positions λ_{sp} measured for two crossed polarizations as a function of gap spacing. Note that the gap values are the designed ones and that all the spectra where background subtracted. The black data points (circle) show $\Delta\lambda$ for antenna dimers oriented along x-direction (parallel to the electrodes), whereas the red data points (square) are for dimers along the y-direction (perpendicular to the electrodes). The data point labeled with a star is the reference antenna constituted of a single element.

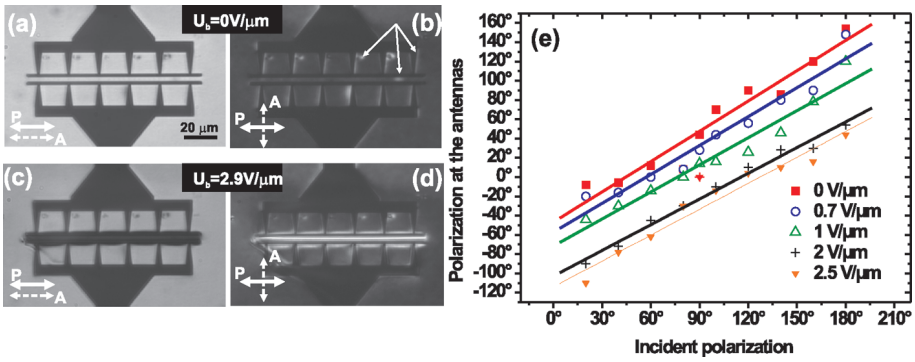

Figure 3. (a,b) Bright-field images of the unbiased cell for (a) collinear polarizer (P, thick arrow) and analyzer (A, dashed arrow) and (b) crossed orientations. (c,d) Same configuration for a static electric field $U_b = 2.9$ V/μm. (e) Polarization direction seen by the antennas as a function of incident polarization and for four cell biases. 0° corresponds to the x-direction.

Consequently, its polarization sensitivity does not significantly vary between the two polarizations ($\Delta\lambda^{ref} = 3$ nm). For coupled disks forming dimer antennas, the plasmon response features the well-known longitudinal (λ_{sp}^{L}) and transverse (λ_{sp}^{T}) plasmon modes of an effective nanorod[24,25] and becomes sensitive to the incoming polarization as shown by the increasing values of $\Delta\lambda$. For the largest separations between the elements (gap >40 nm), the interaction strength is reduced and the weakly coupled dimers behave as individual nanodisks whereby $\Delta\lambda$ is approaching $\Delta\lambda^{ref}$. The difference between the two curves for gap size around 30 nm is attributed to difference in antenna geometry resulting from the limited reproducibility inherent to the fabrication procedure. Figure 2b shows the evolution of the surface plasmon resonance of a dimer antenna when the incoming polarization is systematically varied. The data were obtained for a dimer antenna oriented along the x-direction (parallel to the electrodes). The polar plot shows a monotonous wavelength shift of the surface plasmon resonance between the extremum values (x and y-polarizations).The two eigenmodes are spectrally close to each other and we observe in Figure 2b a result of a linear combination of the two eigenmodes whose respective weight depends on the incident polarization.[26] This behavior is expected considering that the wavelength difference between λ_{sp}^{L} and λ_{sp}^{T} (ca. 20 nm) is smaller than the breadth of the resonance (ca. 70 nm) and the two peaks are undiscernible.

Next, the fabricated antennas were immersed in a liquid crystal (LC) cell (E7 from Merck) in order to modify their dielectric load. The nematic liquid crystal E7 is characterized by a large positive anisotropy (ordinary index $n_o = 1.521$ and extraordinary index $n_e = 1.746$ at 589 nm[27]) permitting thus to significantly alter the antenna surrounding by controlling the orientation of the LC director. The overall thickness of the LC cell was approximately 6 μm.

To verify the homogeneity of the LC and the possible presence of domains between the electrodes, bright-field transmission polarization microscopy was performed with the help of a polarizer (P) and an analyzer (A). Figure 3a,b shows images of an unbiased cell for two crossed positions of the analyzer. In Figure 3a, both polarizer and analyzer are oriented along the x-axis. The electrode system is well recognized. Because of their low optical cross sections, antennas are not visible in this bright-field transmission image. With $P \parallel A$, the optical contrast is positive (bright) indicating that the cell did not introduce a change of polarization. This is confirmed by Figure 3b where $P \perp A$ resulting in an extinction of the transmitted light. We verified that the extinction condition was always obtained for orthogonal P and A regardless the original orientation of the polarizer for an unbiased cell (data not shown). This implies that the linearity of the polarization was not significantly altered by passing through the cell. In these two images, the optical contrast has a good homogeneity across the entire field of view (between the electrodes and outside of the electrode system) indicating a constant orientation of the directors. Small contrast differences are visible at some peculiar areas nearby the electrodes (arrows), but no large-scale macroscopic domains or domain walls are visible within our measurement area (dash boxed in Figure 1).

We did not use any prealignment layer[20] in our experiment as the typical thickness of this layer is comparable to the height of the fabricated antennas (~50 nm). Embedding the antennas in such medium would have considerably reduced the exposed surface and therefore their interaction with the LC molecules. Anchoring of the LC molecules on a glass substrate is mostly homeotropic, that is, normal to the surface.[28] The images of Figure 3a,b agree with this hypothesis since for a homeotropic alignment, the incident light wave travels through a constant n_o index. The alignement of the LC director on gold nanoantenna is also a priori not known since the Au particles were not prefunctionalized[29,30] and different alignment symmetries can be considered.[31,32]

Figure 3c,d show bright field images obtained with the same combinations of P and A but for a cell biased with an electric field $U_b = 2.9$ V/μm. To avoid electrophoresis of the LCs, the applied electric field was alternating with a square waveform at 1 kHz frequency. For $P \parallel A$ (Figure 3c), the optical contrast remains the same as in Figure 3a in equipotential regions (outside the electrodes). However, between the electrodes, where the antennas are, the contrast is reversed (extinction) indicating that the LC director is reoriented and is aligned along the field lines (y-direction). As expected, a bright contrast is observed in Figure 3d when the analyzer is aligned with the applied electric field indicating that the incident light undergoes a significant

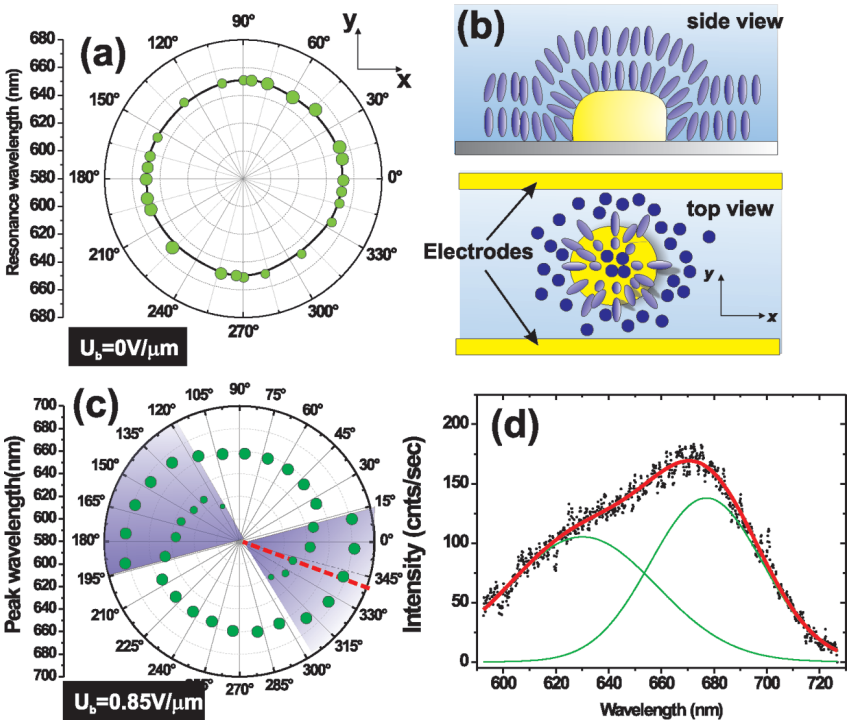

Figure 4. (a) Polar plot of the surface plasmon resonance of the reference disk nanoantenna in the presence of LCs at $U_b = 0$ V/μm. (b) Schematic representations of the orientation of the LC directors on the gold antennas. (c) Response of the same reference antenna when the LCs are oriented by $U_b = 0.85$ V/μm. (d) Scattering spectra corresponding to the polarization indicated by the dashed line in panel c. The solid line is the result of a two-peak Gaussian fit to the experimental data. The amplitude of the peaks are encoded in the size of the symbols

reorientation of its polarization state in the 3.5 μm wide region situated between the electrodes. Elsewhere, the optical contrast is comparable to Figure 3b; the director is not affected by the electric field U_b.

This conclusion implies that when the cell is biased, the polarization experienced by the antennas after passing through the 6 μm thick cell is modified from the polarization incident on the cell. Since the field lines joining the two planar electrodes are not homogeneous across the thickness of the cell, it is difficult to estimate the induced polarization shift acquired by the light upon traveling through the cell thickness (~6 μm). Because of the intrinsic anisotropy of the antenna (dimers) and the anisotropy of the load medium, it is meaningful to know the direction of the polarization as seen by the antennas rather than knowing the state of polarization before the cell. To this aim, we developed a confocal-type microscope[33] constituted of a diascopic objective (numerical aperture, N.A. = 0.65) focusing a 633 nm wavelength laser in ~600 nm spot size placed at equal distance from the electrodes between two sets of antenna. The transmitted intensity through the cell is collected by a high-N.A. objective (N.A. = 1.45). A polarizer and an analyzer were included to measure the transmitted intensity as a function of incident polarization and bias electric field U_b. The result of this analysis is displayed on the graph of Figure 3e for a selection of five biases U_b. The straight lines are linear regressions through the data points. Figure 3e assumes that the polarization analyzed at the exit of the cell corresponds to the polarization seen by the antennas. Since the antennas are fabricated directly on the substrate, we are neglecting any significant polarization shift of the light through a thickness of the cell corresponding to the height of the antennas. We have also assumed that the Δn is not dispersive in the wavelength range considered in the following [500 nm−800 nm].[34] With the help of Figure 3e, the direction of the polarization at the location of the antennas can be retrieved for any incident polarizations and cell biases. We also note that the polarization ratio is affected by the LC molecules. For $U_b = 2$ V/μm, we measured an averaged 7:1 ratio between the intensity analyzed parallel and perpendicular to the polarization. Importantly, in the remainder of this article, the polarization direction is referred to the polarization experienced by the antennas and not the incident polarization on the cell.

Our first experiment consisted at measuring the evolution of the surface plasmon resonance of a single reference disk antenna similar to the one introduced in Figure 2a as a function of polarization, that is, the response of an isotropic particle in an anisotropic medium. Like in Figure 2, dark-field spectroscopy was used to retrieve the scattering properties of the antennas. The result for the reference antenna is displayed in Figure 4a for an unbiased cell. The polar plot indicates a surface plasmon resonance that does not depend on the polarization for $U_b = 0$ V/μm, a trend measured for a series of disk antennas. This finding implies either a random orientation of the LC director with a mixture of planar and normal orientations or a quasi-homeotropic alignment as depicted in Figure 4b. The term *quasi* is used here, because near-neighbor influence (nematic phase at room temperature[35]) prevents a perfect normal-to-the-surface alignment of the directors, and a residual pretilt of the LCs on the surface of high curvatures is probably occurring. A random alignment

on the antenna surface is also unlikely considering that the orientation of a molecule is influenced by its neighbors. Nanosize domains of changing orientations are also not probable as they would involve only a few molecules on the surface of the antenna and would vary in size and orientations between different antennas. From the surface plasmon response of the reference antenna, we hypothesize that Figure 4b is a plausible orientation geometry for an unbiased cell. This statement is in contrast with the expected alignment morphologies theoretically considered by Park and Stroud[31] for which a splitting of the resonances was calculated at a null bias. This is also drastically different from the experimental work of Müller et al. where a clear wavelength shift was measured for a spherical particle.[19] In these two studies however, a prealignment layer was used to anchor the LC director either on the surface of the particle itself[31] or in the plane of the substrate prior to deposit colloidal nanoparticles.[19] These prealignement configurations contributed to the anisotropic response reported at null bias.

Figure 4c shows the surface plasmon resonance trend of the same reference antenna when a weak electric field is applied between the two electrodes ($U_b = 0.85$ V/μm). The polar plot can be divided into two type of angular regions, a range of polarization directions where the antenna features a single resonance and regions for which a resonance peak is observed flanked with blue-shifted shoulder (shaded areas in Figure 4c). An example of a resonance and its shoulder is shown in Figure 4d for a polarization oriented at 340°. The solid line is a two-peak fit to the data with a Gaussian line shape (green lines). The amplitudes of the resonance and the shoulder are encoded in the size of the symbols.

For polarizations comprised between [15°; 120°] and [210°; 300°], the position of the surface plasmon stays constant at 657 nm ± 2 nm and is almost at the same wavelength as the one measured for $U_b = 0$ V/μm (650 nm ± 2 nm). This implies that the index of refraction did not change for these polarizations, that is, the LC directors kept their nominal orientations. The exact position of the resonance is most likely dictated by a linear combination of the indices $\alpha n_o + \beta n_e$, where α and β are weighted coefficients depending on the exact orientation of the LC directors.

For polarizations comprised in the shaded areas, the surface plasmon response is split into two contributions; one is red shifted from the resonance position measured at $U_b = 0$ V/μm, and the second one takes the form of a shoulder located on the blue side of the spectrum. The splitting of the plasmon resonance into two spectral features was, to the best of our knowledge, not observed for an out-of-plane orientation of the LC director on spherical particles.[19] The maximum separation occurs for a direction 165° ↔ 345°. This direction is not aligned with the field lines (90° ↔ 270°) since under this modest bias condition the directors are not fully aligned. We were not able to measure the plasmon responses of the reference antenna for $U_b > 1$ V/μm. Light scattering occurring at the edge of the electrode system for higher electric fields severely reduced the dark-field contrast of the reference antenna (see for instance the arrows in Figure 3b, top right image).

The two spectral features indicate that the surface plasmon response of an isotropic antenna immersed in a anisotropic medium differs from an anisotropic antenna placed in an isotropic medium (Figure 2b). The average depolarization ratio under this polarization range is 17:1 clearly not sufficient to introduce a significant component perpendicularly to the polarization axis. We understand the appearance of the blue shifted shoulder as a signature of a quadrupolar resonant mode. The fact that the shoulder is appearing under an electrical bias implies a n_e dependence. For the shaded areas in Figure 4c, the effective wavelength (λ_{eff}) is reduced by the large value of the index of refraction ($\lambda_{eff} = \lambda_o/n_e$), and quadrupolar resonances may occur. This effect is not observed for a null electric field because the response of the ~100 nm diameter antenna results from a refractive index averaged over all the homeotropic orientations of the directors on the surface. Furthermore, the combination of a dark-field annular illumination at large angle of incidence (0.85 < N.A. < 0.95) together with broken symmetry to the LC reorientation also provides the necessary field overlap to excite quadrupolar modes.[36] The effect of the reorientation of the LC director for $U_b = 1$ V/μm is weaker for polarization range oriented with the applied electric field since the directors are already aligned with U_b. The polarization response of the resonance has a 2-fold symmetry. This is somewhat surprising since the homeotropic directors oriented along the x-axis can flip either way to orient with U_b and should results in a 4-fold symmetry of the polar plot. However, the existence of a pretilt angle would impose a preferred orientation direction that we think is at the origin of the orientation seen in Figure 4c.

A question arising at this point is how many layers are contributing to the formation of the red-shifted peak? The range of interaction of the surface plasmon field is 15−30 nm in air.[33,37,38] A slightly larger interaction range is expected for higher dielectric environment. The length of a E7 molecule is about 2−3 nm,[28] so the surface plasmon will be sensitive to about 10 monolayers of LC molecules.[29]

After characterizing the reference antenna, the influence of the electrical command of the LC on dimer antennas was interrogated. This configuration corresponds to an anisotropic antenna immersed in an anisotropic load medium. We anticipate that the effect of the LC directors on a dimer optical antenna is 2-fold. On the one hand, the λ_{sp}^{L} and λ_{sp}^{T} plasmon modes will be affected by the relative orientation of the n_e and n_o indices. This effect is similar to the one observed for the reference antenna (Figure 4). On the other hand, the interaction strength between the two nanoparticles constituting the dimer antenna will be modulated by the value of the refractive index within the feed-gap area.[39,40] This can be qualitatively understood by the fact that optical fields tend to be less confined in higher dielectric medium and have therefore a longer penetration length in the medium. For a fixed distance between the pair of antennas, a higher refractive index will thus increase the coupling magnitude and introduces a red-shift of the resonances.

Figure 5a−c are polar plots showing the evolution of the surface plasmon resonances of a single dimer antenna as a

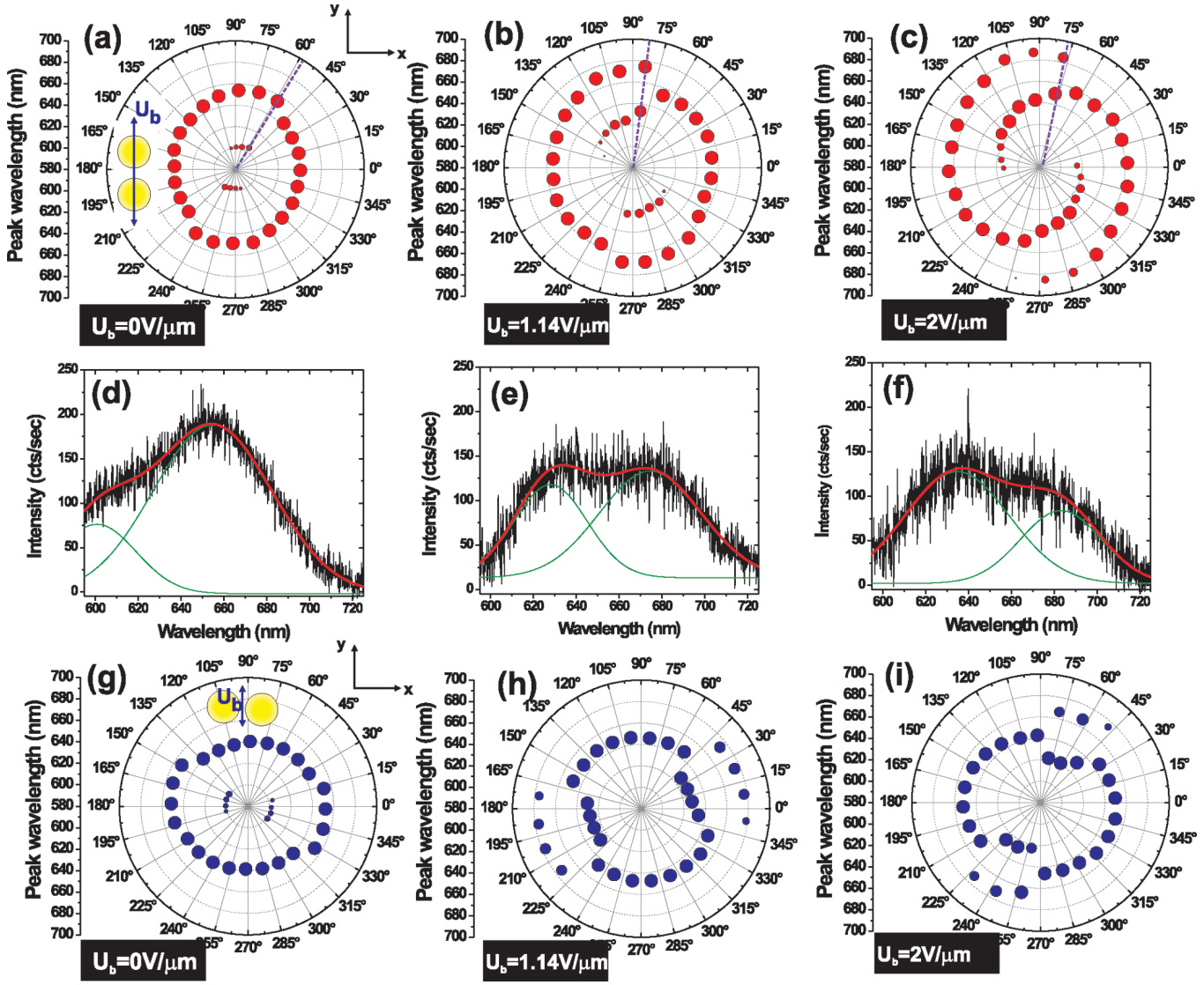

Figure 5. (a−c) Polar plots of the surface plasmon resonances of a dimer nanoantenna in the presence of LCs at respectively $U_b = 0$ V/μm, $U_b = 1.14$ V/μm, and $U_b = 2$ V/μm as a function of polarization. The dimer is aligned with the *y*-direction (90° ↔ 270°). (d−f) Scattering spectra and their two-peak Gaussian fits corresponding to the dashed lines in the polar plots [58° for (a), 82° for (b), and 77° for (c)]. (g−i) Polar plots for a dimer aligned with *x*-direction (0° ↔ 180°) under the same experimental conditions. The amplitude of the peaks are encoded in the size of the symbols.

function of polarization for increasing biases $U_b = 0$ V/μm, $U_b = 1.14$ V/μm, and $U_b = 2$ V/μm, respectively. The value of 1.14 V/μm corresponds to a voltage threshold for which the polar plots were significantly modified by the LC directors possibly indicating a transition between two stationary states (Fréedericksz's transitions[41]). The value of $U_b =$ 2 V/μm is a plateau value from which the resonances are weakly evolving with the maximum applied field (2.9 V/μm). Since a nonconductive substrate was used, accurate measurement of the separation distance was difficult to obtain by electron microscopy. Dark-field microscopy of the dimer in air showed that the particle pair was in optical interaction (similar to Figure 2b) and the edge-to-edge distance was therefore below 40 nm.[24]

The main axis of the optical antenna is aligned with the field lines (*y*-direction; 90° ↔ 270°). The situation for this dimer at a null bias, Figure 5a, is different from a pair of particles in air, Figure 2b. While longitudinal and transversal resonances of the interacting dimer antenna are distinctly marked ($\lambda_{sp}^{L} = 652$ nm and $\lambda_{sp}^{T} = 640$ nm), the scattering spectra in the presence of LC feature a blue-shifted shoulder for polarizations oriented along the main axis. An example of which is shown in Figure 5d for a polarization at 58° together with a two-peak Gaussian fit. For a null bias, this blue-shifted peak is always weaker in magnitude than the main resonance. Here too the respective amplitude of the spectral features are encoded in the symbol size. Since the dimer is immersed to a high-dielectric medium, the dimension of the dimer (ca. 200−300 nm along the long axis) retardation cannot be neglected even for the unbiased cell. Consequently, we also assigned the blue-shifted shoulder of the dimer's response to a quadrupolar mode.

For increasing bias, the position of the spectral signature starts to form a spiral geometry. The spiral shape is better defined with increasing U_b (Figure 5b,c). The averaged polarization ratio for $U_b = 2$ V/μm was above 7:1. This value

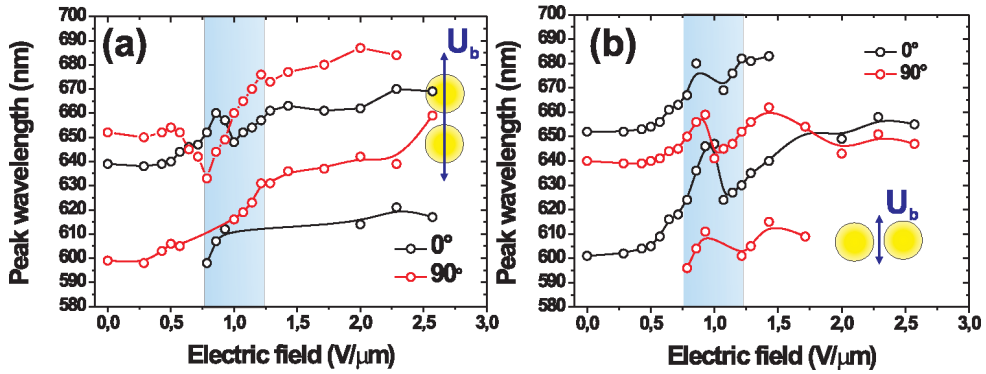

Figure 6. Spectral position of the resonances (data points) as a function of biasing condition for the two polarizations 0 and 90° for an optical dimer antenna oriented parallel (a) or perpendicular (b) to the field lines, respectively. The solid lines are a guide for the eyes and do not constitute an extrapolation of data.

is not sufficient to account for a significant projection of the incident field on the axis. The spiral is therefore linked to the local orientation of the LC molecules on and around the optical antenna. This sensitivity is confirmed by a similar red-shifting of both spectral features as a function of U_b while maintaining their spectral interval constant at $\Delta\lambda = 49 \pm 4$ nm. Because the two particles are in a relative mutual interaction through the feed-gap, their sensitivity to the dielectric environment is enhanced.[39] The position of the resonances follow a monotonous dependence with the incoming polarization and are thus directly related to an inhomogeneous orientation of the directors on the antenna (uncomplete reorientation).

According to the orientation of this particular dimer, the LC directors within the gap separating the two constitutive nanoparticles are aligned with the field lines. Consequently, for a polarization orientation parallel to the applied bias, the optical interaction between the two nanoparticles is enhanced due to the large index of refraction,[39] here n_e. This increased coupling is confirmed by the fact that the longest resonant wavelength is aligned with the long axis of the optical antenna. The amplitude of the resonance decreases for larger wavelength partly because the quantum efficiency of the detectors is reduced after 680 nm. We anticipate a different situation for a dimer antenna orientated perpendicularly to the field lines. In this case, a polarization aligned with the main axis of the antenna will feel a n_o index in the gap, reducing thus the interaction strength between the two nanoparticles.

Figure 5g shows the evolution of the resonances for a single dimer oriented perpendicularly from the one depicted in Figure 5a. The separation between the two particles is nominally the same as the dimer discussed above. Beside the expected 90° shift, the polar plots of Figure 5g and Figure 5a at $U_b = 0$ V/μm show similar trends since the natural orientation of the LC directors on the Au surface should not differ from nanoparticle to nanoparticle. At the transition threshold (1.14 V/μm, Figure 5h), the situation for the two dimers and the reference particle are qualitatively similar; the main resonance is split into two contributions for a certain range of polarization. For the other polarizations in Figure 5h, the resonance features one peak and stays constant at 647 nm $\pm$ 1 nm. Beside an expected angular shift, this behavior is not significantly modified for $U_b = 2$ V/μm. The dipolar and quadrupolar resonances are visible for a polarization range approaching the orientation of the field lines, hence sensing the n_e index. We attribute the remaining angular shift to an uncomplete orientation of the LC directors to a residual anchoring force of the molecules at the surface of the antenna.

Since the two dimers discussed above have the same geometry by design, we attribute the large difference of spectral responses between the two orthogonal antennas (at $U_b = 2$ V/μm) to the orientation state of the LC within the interstitial gap. Controlling the alignment of the director, that is, the antenna load medium, opens the possibility to externally command the electromagnetic interaction between two nanoparticles without modifying their physical separation. Figure 6 shows how this control affects the resonances of the two dimer antennas discussed above. For this graph, the polarization at the particle was fixed at 0 and 90° and U_b was ramped from 0 V/μm to $U_b = 2.9$ V/μm. The presence of Fréedericksz's transitions for electric fields comprised between 0.75 and 1.25 V/μm (blue areas) is obvious from the complex polarization and field dependence of the surface plasmon resonance and the appearance and disappearance of scattering maxima. The small difference in resonance position that can be observed between two extreme values of the applied electric field (e.g., Figure 6b at 90^o) probably originates from an incomplete orientation of the directors even at the highest voltage. Chu et al.[20] measured a saturation of the LC orientation for field greater than 6 V/μm that is twice our source maximum. The wavelength difference (10 to 20 nm) between the ON and OFF states is consistent with previous studies investigating the surface plasmon shift in LC cells.[19,20,27] We have tested the onset of Fréedericksz's transitions on a series of antennas (data not shown) and found that the threshold electric field for the transition did not significantly vary between antennas and had no systematic dependence with the gap size characterizing the dimer antennas. We have also measured a hysteresis curve of the position of the resonance peaks by sweeping the electric field from 0 V/μm $\rightleftharpoons$ 2.9 V/μm (data not shown) and did not observe significant differences between the two sweeps. These two types of measurement indicate that the onset of Fréedericksz's transitions is

reproducible in space (measured for different optical antennas) and time (subsequent measurements). The reproducibility can be understood from the long-lived state of the transient alignment. The lifetime of the alignment above the Fréedericksz's transition can be stable from seconds to hours depending on the magnitude of the applied field with respect to the transition threshold.[43] The time response of the transition itself is strongly depending on the type of liquid crystal used but can be as fast as a few milliseconds.[44] Operating the device around Fréedericksz's transitions is therefore appealing because of the amount of detuning of the antenna response (shaded area in Figure 6) and can be used for applications where very fast switching of the optical antenna characteristics is not required.

In summary, we have reported an electrical means to control the interaction strength between two metallic nanoparticles forming an optical dimer antenna. The control is obtained by modifying the dielectric medium surrounding the dimer antenna through the adjustment of the in-plane orientation of liquid crystal molecules. The responses of the antennas are strongly dependent on the polarization of the light and the orientation of the controlled electric field lines with respect to the antenna axis. We demonstrated an increased optical interaction if the antenna, the field lines and the polarization are collinear. We found that under a bias condition, dimer antenna behaves like a disk antenna if the geometric axis of the antenna is perpendicular to the field lines and polarization.

Modifying the dielectric environment by an external command gives a direct means to control and tune the load of an optical antenna and consequently impedance-match the device.[22,42] While the complete environment of the dimers (feed-gap and surrounding) was affected in this work, we expect that a local addressing of the feed-gap medium alone would provide a higher degree of control for tuning the antenna. We also note that by applying a time-varying bias, amplitude modulation of the optical antennas can be performed with a bandwidth limited by the liquid crystal switching response.

Acknowledgment. The authors thank the Agence Nationale de la Recherche (ANR), under Grants Antares (PNANO 07-51) and Photohybrid (BLANC 07-2-188654) as well as the Regional Council of Burgundy (program FABER) for funding. C.H. acknowledges a stipend from the People's Republic of China. G.P.W. acknowledges support from the U.S. Department of Energy, Office of Science, Office of Basic Energy Sciences, under Contract No. DE-AC02-06CH11357.

References

(1) Bharadwaj, P.; Deutsch, B.; Novotny, L. *Adv. Opt. Photonics* **2009**, *1*, 438–483.
(2) Choi, M.-R.; Stanton-Maxey, K. J.; Stanley, J. K.; Levin, C. S.; Bardhan, R.; Akin, D.; Badve, S.; Sturgis, J.; Robinson, J. P.; Bashir, R.; Halas, N. J.; Clare, S. E. *Nano Lett.* **2007**, *7*, 3759–3765.
(3) Schuck, P. J.; Fromm, D. P.; Sundaramurthy, A.; Kino, G. S.; Moerner, W. E. *Phys. Rev. Lett.* **2005**, *94*, 017402.
(4) Catchpole, K. R.; Polman, A. *Opt. Exp.* **2008**, *16*, 21793–21800.
(5) Tang, L.; Kocabas, S. E.; Latif, S.; Okyay, A. K.; Ly-Gagnon, D.-S.; Saraswat, K. C.; Miller, D. A. B. *Nat. Photonics* **2008**, *2*, 226–229.
(6) Alda, J.; Rico-Garcia, J.; Lopez-Alonso, J.; Boreman, G. *Nanotechnology* **2005**, *16*, S230.
(7) Cubukcu, E.; Kort, E. A.; Crozier, K. B.; Capasso, F. *Appl. Phys. Lett.* **2006**, *89*, 093120.
(8) Anger, P.; Bharadwaj, P.; Novotny, L. *Phys. Rev. Lett.* **2006**, *96*, 113002.
(9) Kühn, S.; Håkanson, U.; Rogobete, L.; Sandoghdar, V. *Phys. Rev. Lett.* **2006**, *97*, 017402.
(10) Taminiau, T. H.; Stefani, F. D.; Segerink, F. B.; van Hulst, N. F. *Nat. Photonics* **2008**, *2*, 234.
(11) Taminiau, T. H.; Stefani, F. D.; van Hulst, N. F. *Opt. Exp.* **2008**, *16*, 10858–10866.
(12) Leroux, Y. R.; Lacroix, J. C.; Chane-Ching, K. I.; Fave, C.; Felidj, N.; Levi, G.; Aubard, J.; Krenn, J. R.; Hohenau, A. *J. Am. Chem. Soc.* **2005**, *127*, 16022–16023.
(13) Zheng, Y. B.; Yang, Y.-W.; Jensen, L.; Fang, L.; Juluri, B. K.; Flood, A. H.; Weiss, P. S.; Stoddart, J. F.; Huang, T. J. *Nano Lett.* **2009**, *9*, 819.
(14) Olk, P.; Renger, J.; Wenzel, M. T.; Eng, L. M. *Nano Lett.* **2008**, *8*, 1174–1178.
(15) Merlein, J.; Kahl, M.; Zuschlag, A.; Sell, A.; Halm, A.; Boneberg, J.; Leiderer, P.; Leitenstorfer, A.; Bratschitsch, R. *Nat. Photonics* **2008**, *2*, 230–233.
(16) Härtling, T.; Alaverdyan, Y.; Hille, A.; Wenzel, M. T.; Käll, M.; Eng, L. M. *Opt. Express* **2008**, *16*, 12362–12371.
(17) Park, S. Y.; Stroud, D. *Appl. Phys. Lett.* **2004**, *85*, 2920–2922.
(18) Dickson, W.; Wurtz, G. A.; Evans, P. R.; Pollard, R. J.; Zayats, A. V. *Nano. Lett.* **2008**, *8*, 281–286.
(19) Müller, J.; Sonnichsen, C.; von Poschinger, H.; von Plessen, G.; Klar, T. A.; Feldmann, J. *Appl. Phys. Lett.* **2002**, *81*, 171–173.
(20) Chu, K. C.; Chao, C. Y.; Chen, Y. F.; Wu, Y. C.; Chen, C. C. *Appl. Phys. Lett.* **2006**, *89*, 103107.
(21) Evans, P. R.; Wurtz, G. A.; Hendren, W. R.; Atkinson, R.; Dickson, W.; Zayats, A. V.; Pollard, R. J. *Appl. Phys. Lett.* **2007**, *91*, 043101.
(22) Alú, A.; Engheta, N. *Phy. Rev. Lett.* **2008**, *101*, 043901.
(23) Alù, A.; Engheta, N. *Nat. Photonics* **2008**, *2*, 307–310.
(24) Tamaru, H.; Kuwata, H.; Miyazaki, H. T.; Miyano, K. *Appl. Phys. Lett.* **2002**, *80*, 1826.
(25) Nordlander, P.; Oubre, C.; Prodan, E.; Li, K.; Stockman, M. I. *Nano. Lett.* **2004**, *4*, 899.
(26) Ibn El Ahrach, H.; Bachelot, R.; Vial, A.; Lerondel, G.; Plain, J.; Royer, P.; Soppera, O. *Phys. Rev. Lett.* **2007**, *98*, 107402.
(27) Kossyrev, P. A.; Yin, A.; Cloutier, S. G.; Cardimona, D. A.; Huang, D.; Alsing, P. M.; Xu, J. M. *Nano Lett.* **2005**, *5*, 1978–1981.
(28) de Gennes, P. G.; Prost, J. *The physics of liquid crystals*; Clarendon Press: Oxford, 1993.
(29) Koenig, G. M.; Gettelfinger, B. T.; de Pablo, J. J.; Abbott, N. L. *Nano Lett.* **2008**, *8*, 2362–2368.
(30) Wilderbeek, H. T. A.; van der Meer, F. J. A.; Feldman, K.; Broer, D. J.; Bastiaansen, C. W. M. *Adv. Mater.* **2002**, *14*, 655.
(31) Park, S. Y.; Stroud, D. *Phys. Rev. Lett.* **2005**, *94*, 217401.
(32) Koenig, G. M.; Ong, R.; Cortes, A. D.; Moreno-Razo, J. A.; de Pablo, J. J.; Abbott, N. L. *Nano Lett.* **2009,** *9*, 2794–2801.
(33) Huang, C.; Bouhelier, A.; Colas des Francs, G.; Bruyant, A.; Guenot, A.; Finot, E.; Weeber, J.-C.; Dereux, A. *Phys. Rev. B* **2008**, *78*, 155407.
(34) Li, J.; Wu, S.-T.; Brugioni, S.; Meucci, R.; Faetti, S. *J. Appl. Phys.* **2005**, *97*, 073501.
(35) Penterman, R.; Klink, S. L.; de Koning, H.; Nisato, G.; Broer, D. J. *Nature* **2002**, *417*, 55–58.
(36) Schider, G.; Krenn, J. R.; Hohenau, A.; Ditlbacher, H.; Leitner, A.; Aussenegg, F. R. *Phys. Rev. B.* **2003**, *68*, 155427.
(37) Rechberger, W.; Hohenau, A.; Leitner, A.; Krenn, J.; Lamprecht, B.; Aussenegg, F. *Opt. Commun.* **2003**, *220*, 137.
(38) Romero, I.; Aizpurua, J.; Bryant, G. W.; García de Abajo, F. J. *Opt. Express* **2006**, *14*, 9988.
(39) Jain, P. K.; El-Sayed, M. A. *Nano Lett.* **2008**, *8*, 4347–4352.
(40) Lassiter, J. B.; Aizpurua, J.; Hernandez, L. I.; Brandl, D. W.; Romero, I.; Lal, S.; Hafner, J. H.; Nordlander, P.; Halas, N. J. *Nano Lett.* **2008**, *8*, 1212–1218.
(41) Fréedericksz, V.; Zolina, V. *Trans. Faraday. Soc* **1933**, *29*, 919–930.
(42) Huang, J.-S.; Feichtner, T.; Biagioni, P.; Hecht, B. *Nano Lett.* **2009**, *9*, 1897–1902.
(43) Winkler, B. L.; Richter, H.; Rehberg, I.; Zimmermann, W.; Kramer, L.; Buka, A. *Phys. Rev. A* **1991**, *43*, 1940–1951.
(44) Kossyrev, P. A.; Qi, J.; Priezjev, N. V.; Pelcovits, R. A.; Craword, G. P. *Appl. Phys. Lett.* **2002**, *81*, 2986–2988.

NL902126Z

PLASMONICS

Tunable resonances

Appl. Phys. Lett. **95,** 154103 (2009)

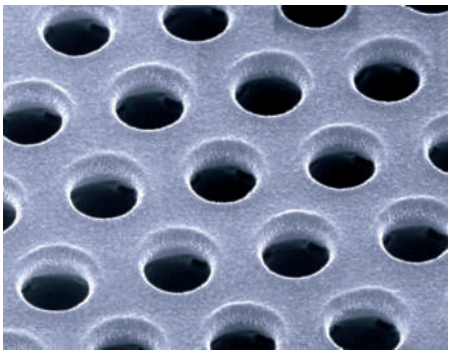

The creation and control of tunable plasmonic properties could be useful for creating new optical filters and metamaterials in the future. Now, unlike previous tuning approaches that have limited spectral range or are based on mechanical processes, the technique demonstrated by Robin Cole and co-workers from the University of Cambridge, UK, is to fabricate metallic nanoscale cavities in a stretchable elastomer film. The attraction of the scheme is that it claims to be a simple, low-cost self-assembly and casting process. A monolayer of polystyrene spheres is first self-assembled on a gold-coated glass slide, and a thin layer of transparent elastomer is drop cast onto the spheres and left to cure. After curing, the elastomer layer is peeled off the substrate with the embedded spheres. The spheres are then removed by dissolving them in dimethylformamide solution. The final stage involves sputtering a 100-nm-thick layer of gold onto the elastomer substrate. As the energy and field distributions of plasmons are dependent on geometry, their properties can be easily tuned by simply applying strain to the structure and stretching it. A plasmonic resonance tunable from 730 nm to 745 nm was achieved at a 5% applied strain. The researchers say that other geometries can also be fabricated.

NONLINEAR OPTICS

Beyond expectations

Opt. Lett. **34,** 3577–3579 (2009)

Waveguides with high-refractive-index materials and subwavelength structures (HIS-WGs) are attractive for a wide variety of nonlinear devices, owing to their strong confinement of light. The nonlinear Schrödinger equation has traditionally been used to describe the propagation of nonlinear pulses in such waveguides, but the weak guidance approximation on which it is based breaks down in the presence of nonlinear effects. Recently, a generalized fully vectorial model of nonlinear pulse propagation was developed by Shahraam Afshar Vahid and co-workers from the University of Adelaide in Australia, and their new description predicted larger values of the effective nonlinear coefficient and Raman gain for HIS-WG structures. Now, the same group has experimentally confirmed that these larger values and the model's calculations are indeed correct for bismuth borosilicate suspended core fibres. The researchers measured the effective nonlinear coefficient of such fibres with diameters of 440, 507, 530 and 555 nm using the dual-continuous-wave method. The results show that the Kerr nonlinearity agrees with the theoretical prediction of the vectorial model in the operating regime of HIS-WGs, confirming the difference in nonlinear coefficients between the standard model and the new model. The researchers attribute this difference to the high-index glass and subwavelength dimension of the fibre used. They say that the new model will help optimize the design and performance of future nonlinear HIS-WGs.

SUPERCONTINUUM GENERATION

From UV to mid-IR

Appl. Phys. Lett. **95,** 161103 (2009)

Supercontinua — ultrabroad bandwidth light pulses usually created by propagating intense optical pulses through a strongly nonlinear media — are attractive for many applications including spectroscopy, optical coherence tomography and the creation of tunable ultrafast femtosecond light sources. So far, however, supercontinuum generation has been limited between UV and near-infrared wavelengths for silica photonic crystal fibres and 0.8–4.5 μm for fluoride fibres. Now, Guanshi Qin and colleagues from Toyota Technological Institute in Japan report that broader operation from the UV to wavelengths as long as 6–8 μm in the mid-infrared can be achieved by using a short length of ZrF_4–BaF_2–LaF_3–AlF_3–NaF fluoride fibre and a high peak pump power. The team investigated a 2-cm-long step-index fluoride fibre with a core diameter of 9 μm, a numerical aperture of 0.2 and a zero-dispersion wavelength of 1.65 μm. Using a 1,450 nm femtosecond laser emitting a peak power of 50 MW as a pump, supercontinuum light with wavelengths ranging from the UV to 6.28 μm was observed. The spectral broadening is said to be a result of self-phase modulation, Raman scattering and four-wave mixing. According to the researchers, the use of a fibre with a larger numerical aperture, such as air-cladding microstructured fibre, could further extend the wavelength to 8 μm.

OPTICAL ANTENNAS

Electrical tuning

Nano Lett. **9,** 3914–3921 (2009)

Johann Berthelot and colleagues from France and the USA have demonstrated active tuning of an optical nano-antenna by electrically controlling its load impedance. The set-up consisted of planar gold electrodes separated by 3.5 μm on a glass substrate, with dimer optical antennas between them. The diameter of the antennas was around 70 nm and they were separated by 0–100 nm. The antennas were submerged in liquid crystals known to exhibit a large anisotropy. Because the optical response of a nanogap antenna is sensitive to changes in the dielectric permittivity of the surrounding material, it is possible to control an antenna's response by manipulating the orientation of the liquid crystals through an external field (provided here by the electrodes). The researchers were thus able to demonstrate polarization-dependent tuning of the

SOLITONS

Dark laser debut

Phys. Rev. A **80,** 045803 (2009)

Although lasers are well known to emit bright pulses of light, a team of researchers in Singapore have now demonstrated the exact opposite — a fibre laser that emits a stream of 'dark pulses'. The erbium-doped fibre laser developed by Han Zhang and co-workers from Nanyang Technological University emits a series of intensity dips in a continuous-wave background of laser emission. The scientists attribute the phenomenon to dark-soliton shaping in the laser cavity. The laser consists of a fibre ring cavity that contains a 5 m length of erbium-doped fibre to provide optical gain and a 150 m length of dispersion compensation fibre. It also features a polarization controller, an isolator, a 50:50 output coupler and a multiplexer for injecting 1,480 nm pump light into the cavity. The researchers observed a series of dark pulses at the fundamental cavity repetition rate. They also say that by carefully controlling the pump strength and orientation of the polarization controller, the output could be reduced to a single dark pulse. Analysis suggests that the dark pulses have a hyperbolic-tangent profile and a typical pulse width of 8 ps, and are transform-limited.

resonance wavelength, obtaining red-shifts up to 50 nm at applied fields of 2.5 V μm^{-1} for particles with resonant wavelengths of ~600 nm. Such effects are needed for the application of nano-antennas in the controlled transfer of optical energy between nanoscale objects.

SILICON PHOTONICS

Mass CMOS production

J. Lightwave Technol. **27,** 4076–4083 (2009)

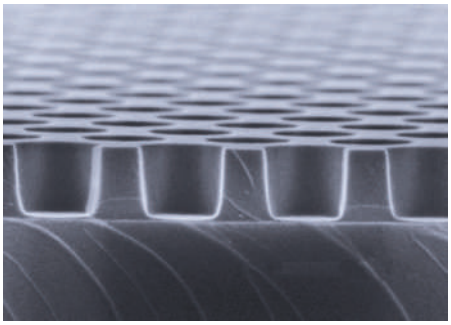

Researchers in Belgium have demonstrated that silicon photonic devices with tolerances of 1% can be fabricated using 193-nm lithography and large-scale CMOS fabrication tools. The main challenge in using lithography to make photonic devices is overcoming the optical proximity effect, which occurs when neighbouring features are very close together, at distances around the illumination wavelength of the lithography process. The image of one structure can interfere with the image of a neighbouring structure, resulting in a change in the light intensity inside the photoresist, which in turn affects the dimensions of the feature.

"The actual optical proximity effect depends on a number of factors, such as the photoresist, bottom antireflective coating thickness, illumination wavelength and the optics of the stepper," explains Shankar Kumar Selvaraja, one of the researchers from the IMEC/Ghent University team. "By choosing a thin photoresist, lower illumination wavelength and better optics, we were able to reduce the proximity effect from 40 nm with a 248 nm process to ~4 nm with a 193 nm process." In a photonic crystal structure, this represents a variation in critical dimensions of only 1%, compared with an industry standard of 5–10% for the fabrication of electronic devices.

Although using a thin photoresist overcame the proximity effect and satisfied resolution requirements, it made transferring the resist pattern into 220 nm of silicon with a dry etch process even more challenging. The team solved this problem by hardening the photoresist using plasma treatment. Another challenge was achieving smooth silicon sidewalls for low propagation loss. "For etching the silicon waveguide we used two gas chemistries and three etch steps, mainly to achieve better uniformity and smooth sidewalls," says Selvaraja. Using this optimized process, the group made photonic wires with a propagation loss as low as 1.8 dB cm^{-1}.

QUANTUM OPTICS

Multiphoton states

Phys. Rev. Lett. **103,** 163602 (2009)

Carefully prepared optical quantum states can be exploited for a host of applications such as quantum computing and metrology. Unfortunately, owing to the probabilistic nature of photons and the complexity of current experimental schemes, engineering entangled states becomes increasingly unfavourable as the number of photons increases. Keven McCusker and Paul Kwiat from the University of Illinois at Urbana-Champaign, USA, propose a new method for preparing multiphoton states. The idea is to drive down-conversion weakly in a cavity until a pair of photons is produced, and then repeat the process to 'build up' a desired state by adding extra photons. By manipulating the polarization of the photon being added or that of the photons already created, it may be possible to produce any state that is expressible as a product of the creation operation. In theory, the performance may exceed state-of-the-art experiments by more than an order of magnitude, but achieving this will require efficient photon detectors and a significant reduction in cavity losses.

SPECTROSCOPY

DUV refractometry

Opt. Express **17,** 18878–18886 (2009)

Biomolecules such as proteins and DNA have distinct absorption spectra at deep-ultraviolet (DUV) wavelengths, which allows accurate measurement of their refractive index and therefore aids their separate quantification. However, their strong absorbance in the DUV region and submicrometre sample size make this measurement challenging. Now, Dan Fu and his co-workers at the Massachusetts Institute of Technology in the USA have proposed a method that can be applied to any wavelength range and suits measurement of both solutions and homogenous objects. The working principle is based on diffraction phase microscopy and the researchers call the scheme field-based light scattering spectroscopy. As a proof of principle, they measured the refractive index dispersion of SiO_2 spheres and protein solutions in the DUV region of 260–315 nm. The SiO_2 spheres, which are approximately 5 μm in size, are immersed in water. The sample solution is sandwiched between two quartz cover slips and located at the beam waist of a DUV beam generated by a femtosecond Ti:Sapphire laser system. The forward scattered beam is diffracted by a grating; the zeroth-order beam is spatially filtered with a pinhole and the first-order beam passes through completely. An interference image is obtained when both the zeroth- and first-order beams reach the CCD camera. The clever part is that because the interference pattern arises from Mie scattering, the size and the refractive index of the spheres can be determined by analysing the observed scattering distribution. The researchers claim that the scheme can determine refractive index with an accuracy better than 0.003.

NANOFABRICATION

Dynamic nanoscribing

Nano Lett. doi:10.1021/nl902682d (2009)

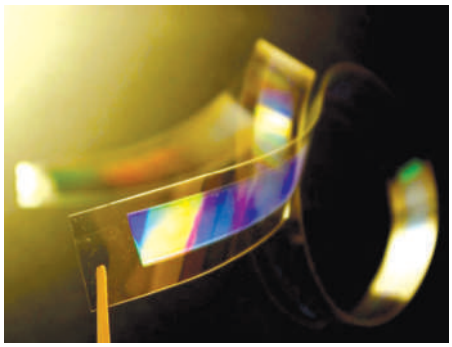

Current laser interference lithography and nanoimprint lithography techniques for fabricating nanoscale structures produce patterns with limited size and require a lengthy processing time (seconds to minutes, depending on the viscosity of the material used). Now, Se Hyun Ahn and Lingjie Jay Guo from the University of Michigan, USA, have demonstrated an elegant solution to these problems — a dynamic nano-inscribing technique. The scheme's operation is analogous to a garden rake creating patterns in soft soil. A patterned rectangular mold made of silicon is angled so that its tip touches the surface of a suitable substrate — composed of indium tin oxide, for example — and is then scanned or dragged across the surface at a speed of up to 10 cm s^{-1}.The sharp edge of the silicon mold inscribes the desired grating patterns. Concentric nanogratings and square-shaped patterns can be fabricated in large areas (for example, the 55.9 cm × 1.27 cm area demonstrated in the experiment) with various nanostructures.